

Robotic Lepidoptery: Structural Characterization of (mostly) Unexpected Palladium Complexes Obtained from High-Throughput Catalyst Screening

John E. Bercaw,^{*,†} Michael W. Day,[†] Suzanne R. Golisz,[†] Nilay Hazari,[†] Lawrence M. Henling,[†] Jay A. Labinger,^{*,†} Susan J. Schofer,[‡] and Scott Virgil[†]

[†]Arnold and Mabel Beckman Laboratories of Chemical Synthesis, California Institute of Technology, Pasadena, California 91125, and [‡]Symyx Technologies, Inc., 1263 East Arques Avenue, Sunnyvale, California 94085

Received March 30, 2009

In the course of a high-throughput search for optimal combinations of bidentate ligands with Pd(II) carboxylates to generate oxidation catalysts, we obtained and crystallographically characterized a number of crystalline products. While some combinations afforded the anticipated (L-L)Pd(OC(O)R)₂ structures (L-L = bipyridine, tmeda; R = CH₃, CF₃), many gave unusual oligometallic complexes resulting from reactions such as C–H activation (L-L = sparteine), P–C bond cleavage (L-L = 1,2-bis(diphenylphosphino)ethane, and C–C bond formation between solvent (acetone) and ligand (L-L = 1,4-bis(2,6-diisopropylphenyl)-1,4-diaza-1,3-butadiene). These findings illustrate potential pitfalls of screening procedures based on assuming uniform, *in situ* catalyst self-assembly.

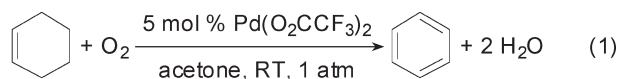
Introduction

The role of automated high-throughput experimentation (HTE) in homogeneous catalysis is steadily increasing.^{1,2} Efficient application of such methods virtually requires some degree of catalyst self-assembly; having to presynthesize all the candidates to be tested will almost always be far too time-consuming. Most commonly members of a ligand library are allowed to react *in situ* with a suitable metal complex, which acts as the catalyst precursor. While this is often successful, there is an obvious concern: in any given case, the targeted species might *not* form, so that a negative result in catalytic performance could reflect that failure rather than the actual properties of the desired catalyst.

On the other hand, in HTE, reactions are often carried out in multiwell plates, with the individual containers more or less open to the environment, thus permitting gradual concentration by solvent evaporation; variations of relative and absolute concentrations, solvent, and temperature may also be included in the screening regime. These constitute excellent conditions for the serendipitous generation of crystals—of the intended product or something else—without much (or any) additional effort. Long ago, Cotton summed up the then-state-of-the-art in characterizing metal cluster structures: “Thus the student of cluster chemistry is in somewhat the position of the collector of lepidoptera or meteorites, skipping observantly over the countryside and exclaiming with delight when fortunate enough to encounter a new

specimen.”³ In this sense, one potential role of an HTE robot may be as an extremely effective butterfly net.

We have recently reported the palladium-catalyzed oxidative aromatization of cycloolefins, using molecular oxygen as the terminal oxidant: cyclohexene can be oxidized to benzene, and 1,2-dihydronaphthalene to naphthalene, at room temperature in the presence of palladium(II) trifluoroacetate (tfa) and O₂ (eq 1).⁴ Palladium complexes with diimine ligands have also been found to oxidatively aromatize cyclohexene to benzene, at elevated temperatures.⁵ For both of these systems, C–H bond activation from an η²-olefinic intermediate is proposed.



We wanted to extend these promising results to the oxidation of more useful substrates such as linear alkenes and alkanes, for which no examples of reaction were found under the above conditions. While the ligand-free Pd(tfa)₂ catalyst system is more active than those of the diimine-ligated complexes, it is also considerably less stable, decomposing to Pd metal at temperatures much above ambient. Conceivably an appropriately ligated catalyst, even if inherently less reactive, could be operated at sufficiently high temperature to overcome the differential and activate more difficult substrates. To explore this possibility, we initiated a

*Corresponding author. E-mail: bercaw@caltech.edu; jal@caltech.edu.

(1) Jäkel, C.; Paciello, R. *Chem. Rev.* **2006**, *106*, 2912–2942.
(2) de Vries, J. G.; de Vries, A. H. M. *Eur. J. Org. Chem.* **2003**, *799*–*811*, and references therein.
(3) Cotton, F. A. *Q. Rev. Chem. Soc.* **1966**, *20*, 389–401.

(4) Bercaw, J. E.; Hazari, N.; Labinger, J. A. *J. Org. Chem.* **2008**, *73*, 8654–8657.

(5) Williams, T. J.; Caffyn, A. J. M.; Hazari, N.; Oblad, P. F.; Labinger, J. A.; Bercaw, J. E. *J. Am. Chem. Soc.* **2008**, *130*, 2418–2419. Bercaw, J. E.; Hazari, N.; Labinger, J. A.; Oblad, P. F. *Angew. Chem., Int. Ed.* **2008**, *47*, 9941–9943.

Table 1. Crystal and Refinement Data for Complexes 1, 2, 3, and 4

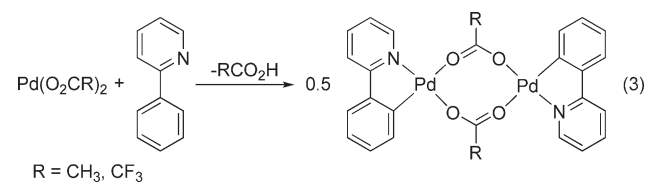
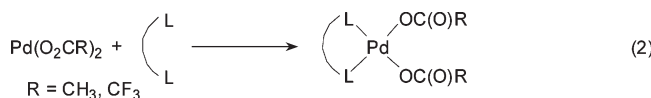
	1	2	3	4
empirical formula	C ₁₄ H ₈ F ₆ N ₂ O ₄ Pd·C ₃ H ₆ O	C ₁₄ H ₁₄ N ₂ O ₄ Pd·5(H ₂ O)	C ₁₀ H ₁₆ F ₆ N ₂ O ₄ Pd	C ₃₈ H ₆₂ N ₄ O ₈ Pd ₃
fw	546.70	470.75	448.65	1022.12
temperature (K)	100	100	100	100
<i>a</i> (Å)	30.4018(13)	6.8790(3)	8.9413(5)	10.8368(6)
<i>b</i> (Å)	13.6007(6)	12.3760(5)	9.4538(5)	16.3596(9)
<i>c</i> (Å)	18.8208(8)	12.7548(6)	10.2243(5)	23.7139(12)
α (deg)	90	115.183(2)	75.945(2)	90
β (deg)	90	96.790(2)	74.203(2)	90
γ (deg)	90	97.921(2)	72.612(2)	90
volume (Å ³)	7782.1(6)	954.15(7)	781.24(7)	4204.1(4)
<i>Z</i>	16	2	2	4
cryst syst	orthorhombic	triclinic	triclinic	orthorhombic
space group	<i>Pnc</i> 2 (#30)	<i>P</i> ī (#2)	<i>P</i> ī (#2)	<i>P</i> 2 ₁ 2 ₁ (#19)
<i>d</i> _{calc} (Mg/m ³)	1.866	1.639	1.907	1.615
θ range (deg)	1.97 to 32.23	1.80 to 39.31	2.10 to 30.78	1.72 to 37.20
μ (mm ⁻¹)	1.043	1.020	1.271	1.322
abs correction	none	semiempirical from equivalents	none	none
GOF	1.57	1.62	2.19	1.39
<i>R</i> ₁ , ^a <i>wR</i> ₂ ^b [<i>I</i> > 2σ(<i>I</i>)]	0.042, 0.072	0.028, 0.042	0.036, 0.075	0.020, 0.033

$$^a R_1 = \sum \|F_o\| - |F_c\| / \sum |F_o|. \quad ^b wR_2 = [\sum [w(F_o^2 - F_c^2)^2] / \sum [w(F_o^2)^2]]^{1/2}.$$

high-throughput study involving a variety of Pd(II) precursors, chelating ligands, solvents, and reaction conditions. While no effective metal–ligand combination was detected, the study did generate a number of crystalline species. Some of these displayed solid state structures quite different from those expected for simple coordination of ligand to Pd (which may be why catalytically active species were not formed), often resulting from unexpected and unusual reactivity. We report here on these findings.

Results and Discussion

HTE Methodology. The robot was used to generate solutions of a wide range of combinations of catalyst precursor (Pd(tfa)₂ or Pd(OAc)₂), ligand, and substrate (cyclohexene or 1,2-dihydronaphthalene) in acetone (Pd(tfa)₂ and Pd(OAc)₂ have limited solubility in many other solvents, and the control reaction described in eq 1 shows significant solvent dependence, so the choice of solvent was not varied in this work). The following N- and P-centered bidentate ligands were expected to react according to eq 2: 2,2'-bipyridine (bpy), *N,N,N',N'*-tetramethylethylenediamine (tmada), (−)-sparteine, 1,2-bis(diphenylphosphino)ethane (dp), and 1,4-bis(2,6-diisopropylphenyl)-1,4-diaza-1,3-butadiene (diimine). 2-Phenylpyridine was also included in the study, anticipating that a chelate product would result from C–H activation, as shown in eq 3.



When cyclohexene was used as substrate, control samples (without substrate) were found to contain substantial amounts of both cyclohexene and benzene, indicating

considerable cross-contamination by volatile components. Although we expect this problem could have been largely eliminated by improving the experimental setup (which employed a porous rubber mat held flush to the glass vials with a metal plate affixed by screws), instead we simply restricted screening to the less volatile 1,2-dihydronaphthalene, for which no such transfer could be detected. Most ligand–Pd combinations resulted in no oxidation activity whatsoever; a couple of cases gave low activity, substantially less than that found for the ligand-free catalysts. (We believe incomplete complexation is probably responsible for these low conversions; another possibility is that some ligated palladium complexes are active, although inherently less active than their ligand-free counterparts). Hence, this survey was abandoned.

A parallel set of substrate-free samples was generated, using the robot, to investigate whether the desired catalysts assemble properly. In many of these cases, solvent evaporation in air directly provided X-ray quality crystals. All such reactions were scaled up in the laboratory, to determine by NMR spectroscopy whether the crystalline material was identical to the main product generated in solution. Some of the products were also examined by mass spectrometry.

Bipyridine Complexes. Both Pd(tfa)₂ and Pd(OAc)₂ react with bpy according to eq 2, as confirmed by ¹H NMR spectroscopy. From the HTE screening, (bpy)Pd(tfa)₂ (**1**) was obtained as pale yellow needles (crystal and refinement data are shown in Table 1). The inner coordination sphere of **1** (Figure 1) appears entirely unexceptional, with the bipyridine lying in the Pd coordination plane and the two monodentate trifluoroacetate groups bent out of the plane, both in the same direction, very similar to the orientation found in an earlier structure of a (bpy)Pd(carboxylate)₂.⁶ The crystal packing of **1** reveals intermolecular Pd–Pd and π-stacking interactions between adjacent molecules (Figure 2), and the separations fall within the expected range: Pd–Pd distances are between 3.0 and 3.2 Å, and all spacings between the bpy rings are less than 3.8 Å, with the closest contact being approximately 3.4 Å. Each complex participates in a Pd–Pd interaction with another complex directly above (or below)

(6) Canty, A. J.; Denney, M. C.; Skelton, B. W.; White, A. H. *Organometallics* 2004, 23, 1122–1131.

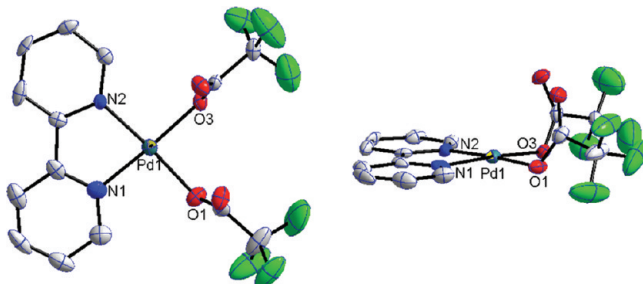


Figure 1. Solid state structure of **1**. Hydrogens have been omitted for clarity. Selected bond distances of **1** (Å): Pd1–N1 2.004(1), Pd1–N2 1.993(1), Pd1–O1 2.016(1), Pd1–O3 2.007(1).

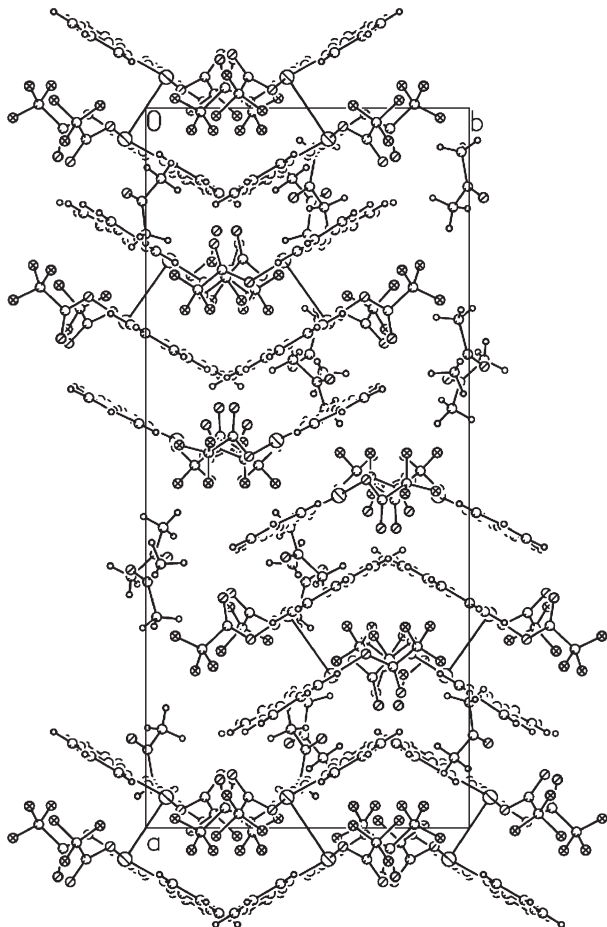


Figure 2. Unit cell diagram of **1** viewed along the *c*-axis.

and a π -stacking interaction between bpy rings with the complex directly below (or above). These two interactions combine to create a columnar structure comprised of alternating d^8 – d^8 and π -stacking interactions. While both π -stacking between adjacent bpy rings⁷ and d^8 – d^8 interactions between metal centers^{8,9} are well established, to the best of our knowledge, **1** is the first example of a structure that contains *both* of these interactions in the same crystal. Another noteworthy feature of the layered structure is the presence of four independent molecules in the unit cell.

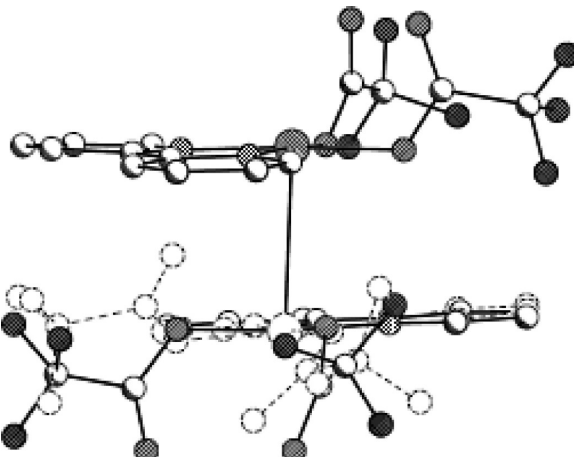


Figure 3. Comparison of the molecular conformation in the two polymorphs of (bpy)Pd(tfa)₂ with **1** as the solid bonds and **1'** as the dashed bonds.

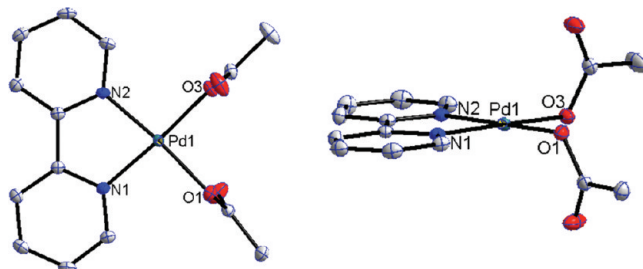


Figure 4. Solid state structure of **2**. Hydrogens have been omitted for clarity. Selected bond distances of **2** (Å): Pd1–N1 1.998(1), Pd1–N2 1.992(1), Pd1–O1 2.013(1), Pd1–O3 2.007(1).

A second polymorph of **1** (**1'**) was also obtained. Although these crystals were not of high enough quality to obtain quantitative data, an overlay of the two molecules shows clear differences (Figure 3). In particular, the trifluoroacetate groups are no longer oriented in the same direction with respect to the square plane as in **1**. This allows the molecules to align in the unit cell so that π -stacking is the predominant interaction, with no short Pd–Pd contacts. For **1**, it appears that such an alignment, with only π -stacking (or only d^8 – d^8 interactions), is prevented by steric repulsions between the parallel-oriented tfa groups. Clearly there is only a small energetic difference between **1** and **1'**, and the exact conditions for crystallization influence which polymorph is obtained.

The yellow crystals of (bpy)Pd(OAc)₂ (**2**) obtained through HTE exhibit a structure very similar to that of **1'** (Figure 4), with the two acetate groups oriented above and below the coordination plane (crystal and refinement data are shown in Table 1). There is a slightly offset face to face π -stacking interaction between the bpy rings of adjacent molecules (shortest contact 3.4 Å) and no evidence for any Pd–Pd interaction.⁷ One notable feature of **2** is a hydrogen-bonded network of waters (not shown), which are also hydrogen bonded to the acetate ligands. This water presumably originates from wet solvents that were used in the reaction.

Tetramethylethylenediamine and Palladium(II) Trifluoroacetate. The reaction of tmeda and Pd(tfa)₂ in acetone also followed eq 2 (confirmed by ¹H NMR spectroscopy), giving colorless crystals of (tmeda)Pd(tfa)₂ (**3**). The structure (Figure 5) is similar to those of **1** and **2** but exhibits

(7) Janiak, C. *J. Chem. Soc., Dalton Trans.* **2000**, 3885–3896.

(8) Roundhill, D. M.; Gray, H. B.; Che, C. M. *Acc. Chem. Res.* **1989**, 22, 55–61.

(9) Connick, W. B.; Marsh, R. E.; Schaefer, W. P.; Gray, H. B. *Inorg. Chem.* **1997**, 36, 913–922.

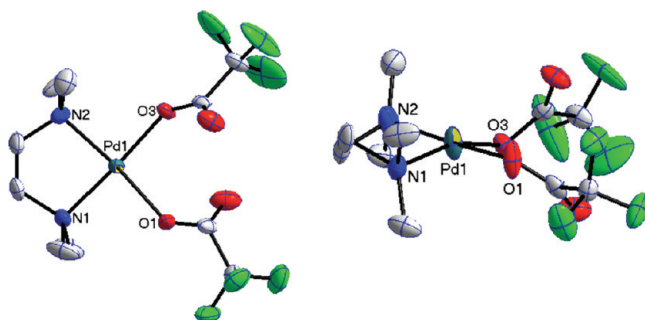


Figure 5. Solid state structure of **3**. Hydrogens have been omitted for clarity. Selected bond distances of **3** (\AA): Pd1–N1 2.017(1), Pd1–N2 2.034(1), Pd1–O1 2.025(1), Pd1–O3 2.079(1) or 2.095(1). (If only one value is given, the distances are the same in both conformations.)

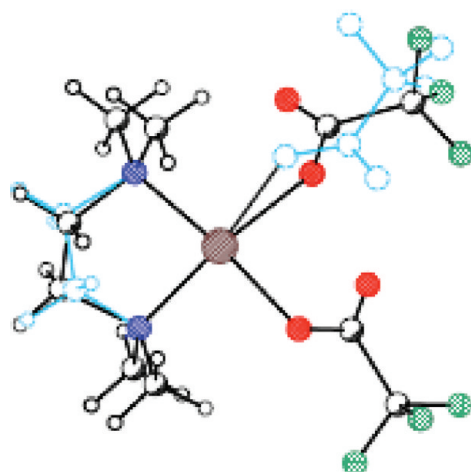


Figure 6. Overlay of the two conformations of **3**.

disorder in both the tfa groups and the ethylene backbone (crystal and refinement data are shown in Table 1). In the two (uncoupled) conformations in this crystal, the carbonyl oxygens of the tfa ligands are on either the same or opposite sides of the coordination plane, and the two carbons of the ethylene backbone of tmeda alternate between being up or down with respect to the coordination plane (Figure 6).

Phenylpyridine Reactions. The reaction of phenylpyridine with both $\text{Pd}(\text{OAc})_2$ and $\text{Pd}(\text{tfa})_2$ gave C–H activation products as expected (eq 3). The yellow crystals of both products exhibit a “clamshell” dimer structure, as reported previously for the acetate complex,^{10,11} in which the two phenylpyridines are stacked on top of each other and the bridging acetates are perpendicular to the palladium–ligand coordination planes. The structure of the tfa complex, which features a relatively short palladium–palladium interaction, will be fully discussed in a subsequent paper describing the electronic structure of d^8 – d^8 bonding in Pd complexes.¹²

(–)-Sparteine and Palladium(II) Acetate. While there are many examples of sparteine acting as an L_2 -type ligand

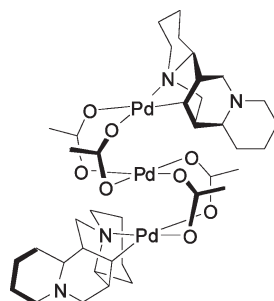


Figure 7. Schematic representation of **4**.

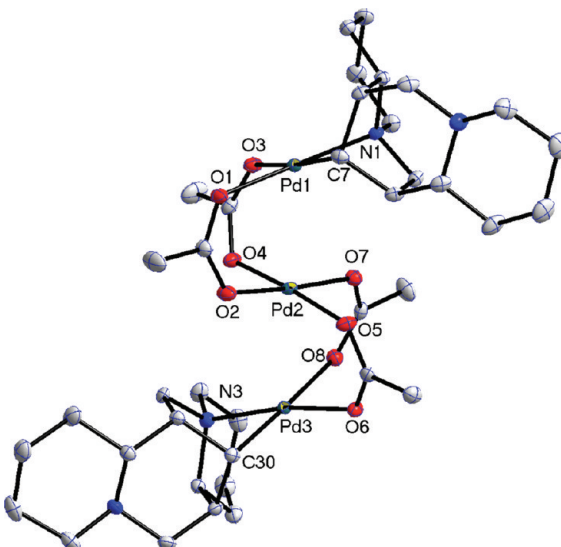


Figure 8. Solid state structure of **4**. Hydrogens have been omitted for clarity. Selected bond distances of **4** (\AA): Pd1–N1 2.061(1), Pd1–C7 2.010(1), Pd3–N3 2.069(1), Pd3–C30 1.997(1).

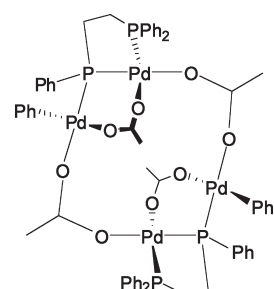


Figure 9. Schematic representation of **5**.

to palladium (eq 2),^{13–16} the gray crystals obtained from mixing (–)-sparteine and $\text{Pd}(\text{OAc})_2$ in acetone instead consist of (sparteinyl) $\text{Pd}(\mu\text{-OC}(\text{CH}_3)\text{O})_2\text{Pd}(\mu\text{-OC}(\text{CH}_3)\text{O})_2\text{Pd}$ –(sparteinyl) (**4**), the result of C–H activation at a bridgehead position of sparteine (crystal and refinement data are shown in Table 1). The resulting trimetallic complex contains three palladium atoms (Figures 7 and 8), in an approximately linear

(10) Thu, H.-Y.; Yu, W.-Y.; Che, C. M. *J. Am. Chem. Soc.* **2006**, *128*, 9048–9049.

(11) Dincer, M.; Ozdemir, N.; Gumar, M. E.; Cetinkaya, B. *Acta Crystallogr. Sect. E: Struct. Rep. Online* **2008**, *E64*, m381.

(12) Bercaw, J. E.; Durrell, A. C.; Gray, H. B.; Green, J. C.; Hazari, N.; Labinger, J. A.; Winkler, J. R., manuscript in preparation.

(13) Togni, A.; Rihs, G.; Pregosin, P. S.; Ammann, C. *Helv. Chim. Acta* **1990**, *73*, 723–732.

(14) Trend, R. M.; Stoltz, B. M. *J. Am. Chem. Soc.* **2004**, *126*, 4482–4483.

(15) Intini, F. P.; Pacifico, C.; Pellicani, R. Z.; Roca, V.; Natile, G. *Inorg. Chim. Acta* **2008**, *361*, 1606–1615.

(16) Mueller, J. A.; Sigman, M. S. *J. Am. Chem. Soc.* **2003**, *125*, 7005–7013.

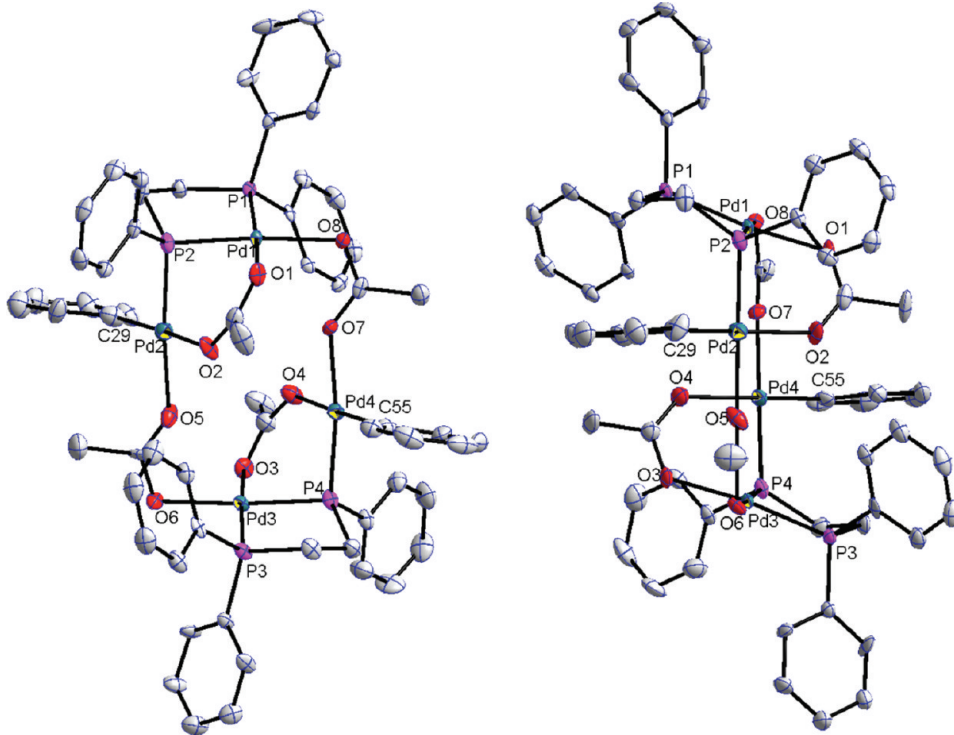


Figure 10. Solid state structure of **5**. Hydrogens have been omitted for clarity. Selected bond distances of **5** (Å): Pd1–P1 2.215(1), Pd1–P2 2.214(1), Pd1–O1 2.080(1), Pd1–O8 2.145(1), Pd2–P2 2.240(1), Pd2–C29 1.973(1), Pd2–O2 2.150(1), Pd2–O5 2.153(1), Pd3–P3 2.214(1), Pd3–P4 2.216(1), Pd3–O3 2.084(1), Pd3–O6 2.149(1), Pd4–P4 2.227(1), Pd4–C55 2.004(1), Pd4–O4 2.169(1), Pd4–O7 2.128(1).

Table 2. Crystal and Refinement Data for Complexes **5 and **6****

	5	6
empirical formula	C ₆₀ H ₆₀ O ₈ P ₄ Pd ₄	C ₃₁₀ H ₄₂₈ N ₂₀ O ₃₀ Pd ₁₀ ·8(C ₂ H ₄ O ₂)·2(H ₂ O)
fw	1458.56	6495.17
temperature (K)	100	100
<i>a</i> (Å)	12.8301(6)	12.6109(5)
<i>b</i> (Å)	20.9667(9)	28.7865(11)
<i>c</i> (Å)	21.6140(10)	29.2433(12)
α (deg)	90	113.477(2)
β (deg)	100.018(3)	100.174(3)
γ (deg)	90	93.227(3)
volume (Å ³)	5725.6(4)	9489.3(7)
<i>Z</i>	4	1
cryst syst	monoclinic	triclinic
space group	<i>P</i> 2 ₁ /c (#14)	<i>P</i> 1 (#2)
<i>d</i> _{calc} (Mg/m ³)	1.692	1.137
θ range (deg)	1.91 to 30.44	1.66 to 22.50
μ (mm ⁻¹)	1.402	0.523
abs correction	semiempirical from equivalents	semiempirical from equivalents
GOF	2.96	2.32
<i>R</i> ₁ , ^a <i>wR</i> ₂ , ^b [<i>I</i> > 2σ(<i>I</i>)]	0.072, 0.126	0.079, 0.137

^a *R*₁ = $\sum |F_{\text{o}}| - |F_{\text{c}}| / \sum |F_{\text{o}}|$. ^b *wR*₂ = $[\sum [w(F_{\text{o}}^2 - F_{\text{c}}^2)^2] / \sum [w(F_{\text{o}}^2)^2]]^{1/2}$.

arrangement ($\angle \text{Pd1–Pd2–Pd3} = 176.03^\circ$; $\text{Pd–Pd} \approx 2.9$ Å), each exhibiting square-planar geometry. The central Pd is coordinated to four acetate groups ($\text{Pd–O} \approx 2.0$ Å); these bridge in pairs to the two outer Pds, each of which is additionally coordinated by a (κ^2 -N,C)-sparteinyl group. The sparteinyl ligand has undergone an inversion at one of the nitrogen atoms (relative to free sparteine), presumably to assist with coordination. Overall, the structure of the molecule is S-shaped and seems to involve two d⁸–d⁸ interactions.¹²

When this reaction was performed on a large scale, the presence of **4** as the major product was confirmed by HRMS and ¹H NMR spectroscopy. We are unable to propose a detailed mechanism for formation of **4** at this time, although

presumably the hydrogen generated by C–H activation is released as acetic acid. It is probable that the solvent (acetone) is partially responsible for promoting C–H bond activation, as it has been previously reported that reaction of sparteine with Pd(OAc)₂ in dichloroethane results in the formation of (sparteine)Pd(OAc)₂.¹⁶ To the best of our knowledge, this is the first example of a metal complex containing a metalated sparteine ligand.

1,2-Bis(diphenylphosphino)ethane and Palladium(II) Acetate. The colorless crystals obtained from the mixture of dp and Pd(OAc)₂ in acetone exhibit a tetrametallic structure, $[(\text{Pd}(\mu\text{-PPhCH}_2\text{CH}_2\text{PPh}_2)(\mu\text{-OC(CH}_3\text{)}\text{O})\text{PdPh})(\mu\text{-OC(CH}_3\text{)}\text{O})_2]$ (**5**), resulting from C–P cleavage of the dp ligand

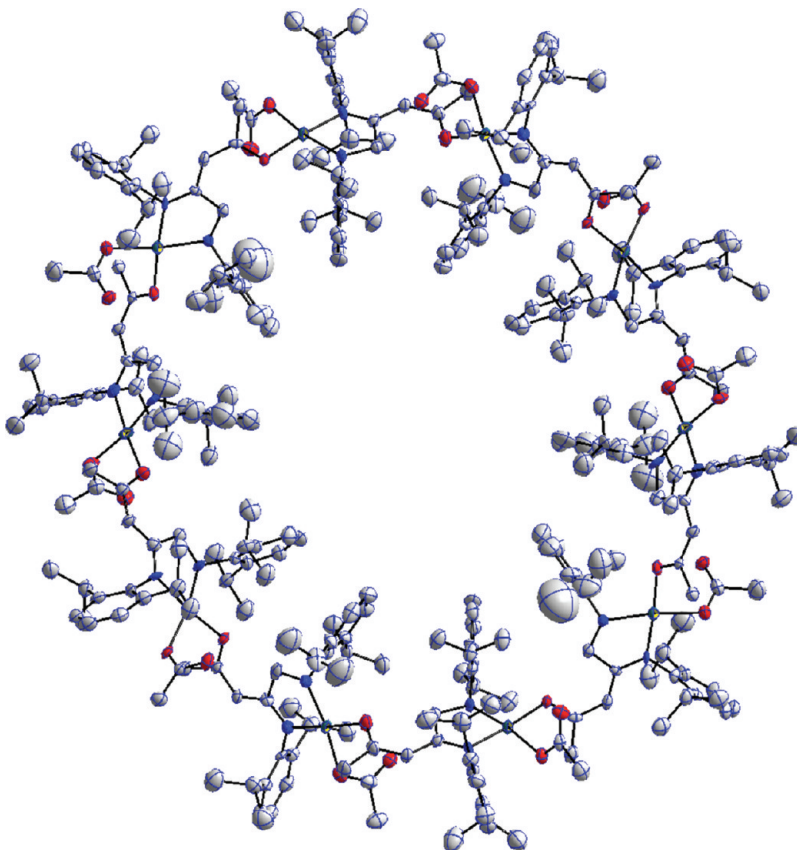


Figure 11. Solid state structure of **6**. Hydrogens have been omitted for clarity. Selected bond distances of **6** are listed in the Supporting Information.

(Figure 9). Two representations of **5** are shown in Figure 10 (crystal and refinement data are shown in Table 2). The four Pd(II) centers are each square planar and are arranged in pairs. One member of each pair (Pd2, Pd4) is bonded to a phenyl group, and the other (Pd1, Pd3) to the intact Ph₂P end of a dp. The other (phosphide) end of the dp, along with one acetate, bridge the two members of each pair; and then the pairs are joined together by two additional bridging acetates (Pd1 to Pd4, Pd2 to Pd3). The overall arrangement is an approximately planar macrocycle containing the four Pd atoms (torsion angle = 0.43°), the two bridging phosphide P atoms, and the two interpair bridging acetates, with the other (intrapair) bridging acetates and the phosphine P atoms above and below the plane.

Repeated large-scale reactions of dp and Pd(OAc)₂ in acetone gave only (dp)Pd(OAc)₂ (**5m**), the expected monomeric product according to eq 2. This complex has been previously reported, along with the crystal structure (which includes a coordinated CH₂Cl₂ molecule).¹⁷ The structural parameters of **5m** were identical to those in the literature, with the replacement of CH₂Cl₂ by half a molecule of acetone in the unit cell (see Supporting Information for crystal and refinement data). We were unable to synthesize **5** on a large scale, and thus designate it as a minor product in the reaction of dp and Pd(OAc)₂.

1,4-Bis(2,6-diisopropylphenyl)-1,4-diaza-1,3-butadiene and Palladium(II) Acetate. The reaction of diimine with Pd(OAc)₂

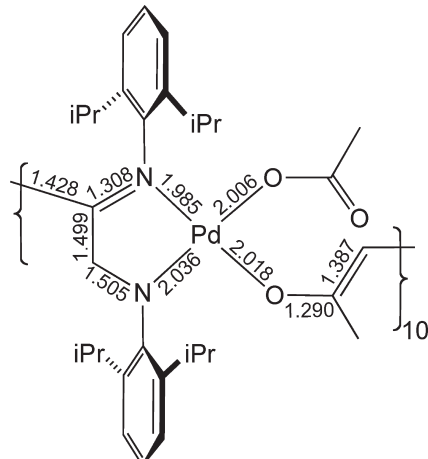


Figure 12. Schematic representation of **6**, showing key bond lengths (values averaged over the five independent units).

in acetone yielded small red crystals, for which X-ray crystallographic studies revealed the remarkable cyclic decameric structure shown in Figure 11 (crystal and refinement data in Table 2). The connections between units involve —OC—(CH₃)X— groups that are O-bound to one Pd and X-attached to a backbone carbon of a diimine ligand on the neighboring Pd. At first we thought that X was either O or CH₂, corresponding respectively to bridging acetate or the enolate of acetone, either of which would give overall charge neutrality. However, closer inspection of the crystallographic data shows

(17) Bianchini, C.; Lee, H. M.; Meli, A.; Oberhauser, W.; Peruzzini, M.; Vizza, F. *Organometallics* **2002**, *21*, 16–33.

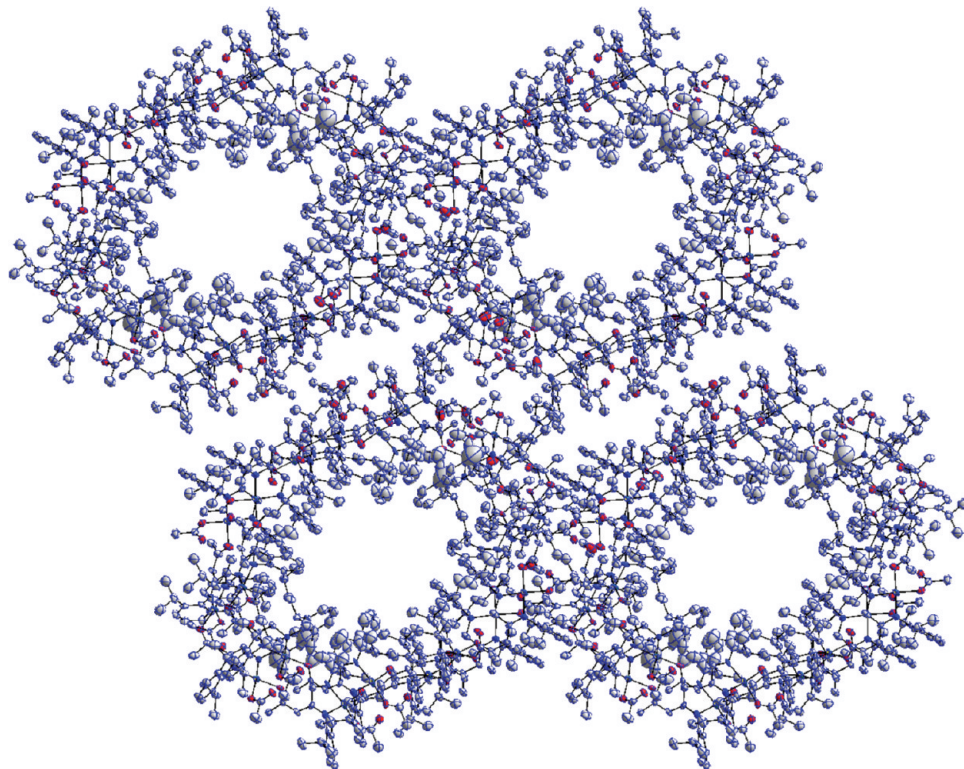


Figure 13. Diagram of the crystal packing of **6**.

clearly that X is in fact a $=\text{CH}-$ group. The structure refines much more poorly with $\text{X} = \text{O}$ than $\text{X} = \text{C}$; electron density peaks corresponding to a single H can be located at the expected positions adjacent to each C; and the relative bond lengths are consistent only with this formulation, as is the ^1H NMR spectrum, which includes signals (all of intensity corresponding to one proton) at δ 4.05 (s), 3.15 (d), and 4.83 (d) for the $=\text{CH}-$ and the two nonequivalent backbone CH_2 protons, respectively. (A parent ion for the intact decamer could not be detected by mass spectrometry, perhaps not surprisingly.) The molecular structure is shown schematically in Figure 12, along with the key bond distances.

Stoichiometrically, the formation of **6** corresponds to net double deprotonation of acetone, with the addition of the carbon end to one of the backbone imine carbons and migration of the hydrogen originally on that carbon to the adjacent carbon; this has taken place 10 times per macrocycle, in which each Pd is square-planar, coordinated by one imine N, one amidic N, one normal (monodentate) anionic acetate, and an O from what has become a substituted acetonyl. Since three of those are anionic ligands, each Pd is anionic; hence there must be one additional proton per Pd that was not crystallographically detected. Most probably those are hydrogen-bonded to the dangling oxygens on the periphery of the macrocycles; alternatively, they may be bonded to solvent and/or water molecules inside the channels that are formed by the stacking of decamers in the crystal packing (Figure 13). There is no covalent bonding between the channels. We were unable to obtain the high-angle diffraction data that would be needed to determine whether any solvent or other molecules are present in the channels, and thermogravimetric analysis was inconclusive, but it seems highly unlikely that they are empty considering the intimate involvement of the solvent.

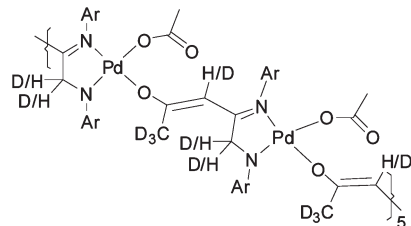


Figure 14. Schematic representation of **6-d_n** showing the sites of H/D scrambling.

It appears that **6** is not merely a minor component of the reaction mixture, as it could be synthesized in reasonable yield (36%) on a large scale. We would expect that a compound of the form (diimine) $\text{Pd}(\text{OAc})_2$ might be an intermediate, and ^1H NMR changes during early stages of the reaction between diimine and $\text{Pd}(\text{OAc})_2$ in acetone- d_6 suggest that is the case. We were subsequently able to isolate (impure) samples of (diimine) $\text{Pd}(\text{OAc})_2$ from the reaction of the diimine ligand and $\text{Pd}(\text{OAc})_2$ in CHCl_3 , and dissolution of isolated (diimine) $\text{Pd}(\text{OAc})_2$ in acetone- d_6 led to the formation of **6-d_n**, as confirmed by X-ray crystallography and ^1H NMR spectroscopy. Detailed comparison of the ^1H NMR spectrum with that for the all-protio analogue (see the Supporting Information) shows that the acetone-derived methyl group is entirely deuterated, but remaining deuterons on the deprotonated end have completely exchanged with the backbone protons of the ligand (Figure 14), as revealed by signals corresponding to both CH_2 and CHD in the methylene position and reduction of intensity for all three of the signals cited above. At present we do not have a mechanistic proposal to account for the formation of **6** and the H/D scrambling process.

Conclusions

While the above findings remind us of the potential pitfalls of screening protocols that rely on catalyst self-assembly, they also illustrate their capability for generating intriguing structures. More than half of the ligand–metal combinations tested afforded products resulting from unexpected chemistry—C–H bond activation, C–P bond cleavage, addition of solvent to ligand—that led to further assembly into oligomeric structures with intricate and unusual interconnections, which (while gladdening the collector’s heart) are less likely to function as effective catalysts. Because the efficiency of HTE screening for homogeneous catalysts relies on some assumed uniformity of catalyst self-assembly, it is important to carry out some structural verifications of (pre)catalysts so generated, for at least representative ligand/metal complex/solvent combinations. Researchers making use of these powerful methodologies should stay alert to both the risks and the opportunities.

Experimental Section

General Considerations. All manipulations were performed in air. Acetone, palladium(II) acetate, palladium(II) trifluoroacetate, (−)-sparteine, 2-phenylpyridine, and tmeda were purchased from Aldrich and used as received. 2,2'-Bipyridine was purchased from Acros Organics and used as received. 1,2-Bis(diphenylphosphino)ethane was purchased from Pressure Chemical Company and used as received. 1,4-Bis(2,6-diisopropylphenyl)-1,4-diaza-1,3-butadiene was prepared by literature methods.¹⁸ Acetone-*d*₆ and chloroform-*d*₃ were purchased from Cambridge Isotopes and used as received. ¹H NMR spectra were recorded on a Varian INOVA 500 MHz instrument using the VNMRJ software program, version 2.2d, at room temperature. Proton chemical shifts were reported using the residual solvent signal as the internal standard. High-resolution mass spectra (HRMS) were obtained from the California Institute of Technology Mass Spectrometry Facility.

High-Throughput Equipment. Experiments were conducted using a Symyx Technologies Core Module robotic system (Santa Clara, CA). The core module was operated with library designs and operating protocols developed using Library Studio software version 7.1.9.50 and Automation Studio version 1.1.1.8. Stock solutions of metal complexes and ligands were prepared at 0.1 M in acetone. The metal solutions were added to the wells followed by an equimolar amount of the ligand solutions. Acetone was ultimately added to each of the wells to keep a constant total volume of 500 μL. Each combination of metal and ligand was performed in quadruplicate, with a concentration gradient for each set of four wells such that the least concentrated contained 5 mmol each of metal and ligand and the most concentrated contained 15 mmol each of metal and ligand. The wells were then left open to the air on the benchtop until crystals formed. Crystal formation was complete in less than 24 h for some complexes.

X-ray Crystallography. The crystals were mounted on a glass fiber with Paratone-N oil. Data were collected on a

Bruker KAPPA APEX II instrument. Structures were determined using direct methods or, in some cases, Patterson maps with standard Fourier techniques using the Bruker AXS software package.

General Procedure for Large-Scale Reactions. In order to confirm whether the crystals formed in the HTE screening were the major products, reactions between metal precursors and ligands were performed on a larger scale in the laboratory. The conditions utilized in the HTE screening were replicated. In the case of reactions between bpy and Pd(tfa)₂, bpy and Pd(OAc)₂, tmeda and Pd(tfa)₂, and dp and Pd(OAc)₂, ¹H NMR spectroscopy was used to monitor the reactions and indicated the clean formation of compounds **1**, **2**, **3**, and **5m**, respectively. The chemical shifts for **1**,¹⁹ **2**,¹⁹ **3**,¹⁴ and **5m**¹⁷ were consistent with those previously reported in the literature.

(sparteinyl)Pd(μ-OC(CH₃)O)₂Pd(μ-OC(CH₃)O)₂Pd(sparteinyl) (**4**). A solution of (−)-sparteine (104 mg, 0.44 mmol) in acetone (4.4 mL) was added to a solution of Pd(OAc)₂ (100 mg, 0.44 mmol) in acetone (4.4 mL). The solution was allowed to evaporate in air to give gray crystals (37 mg, 24% yield), which were filtered from the supernatant before analysis. See SI for ¹H NMR spectrum. HRMS (FAB+): obsd M+ 1021.160, calcd for C₃₈H₆₂N₄O₈Pd₃, 1021.160.

[diimine](Pd)(OAc)(OC(CH₃)CH)]₁₀ (**6**). A solution of diimine (167 mg, 0.44 mmol) in acetone (4.4 mL) was added to a solution of Pd(OAc)₂ (100 mg, 0.44 mmol) in acetone (4.4 mL). The solution was allowed to evaporate in air to give red-orange crystals (94.5 mg, 36% yield), which were filtered from the supernatant before analysis. ¹H NMR (500 MHz, CDCl₃) δ 0.62 (d, *J* = 6, 3H, ⁱPr), 0.82 (m, 6H, ⁱPr), 0.90 (d, *J* = 6, 3H, ⁱPr), 1.00 (s, 3H, ⁱPr*), 1.13 (d, *J* = 6, 3H, ⁱPr), 1.19 (d, *J* = 6, 3H, ⁱPr), 1.22 (d, *J* = 6, 3H, ⁱPr), 1.99 (s, 3H, CH₃), 2.13 (s, 3H, CH₃), 2.90 (m, 1H, CH), 3.05 (m, 1H, CH), 3.15 (d, *J* = 13, 1H, CH₂), 3.61 (m, 1H, CH), 4.05 (s, 1H, CH), 4.45 (m, 1H, CH), 4.83 (d, *J* = 13, 1H, CH₂), 6.60 (d, *J* = 7, 1H, Ar), 6.88 (m, 2H, Ar), 7.03 (t, *J* = 7, 1H, Ar), 7.11 (t, *J* = 7, 2H, Ar). The resonance with an asterisk corresponds to an unknown peak that has appeared in all spectra of all samples of **6**. This unknown is coincident with an isopropyl resonance.

Acknowledgment. The authors acknowledge bp for funding through the MC² program and thank John C. McKeen of Caltech for TGA and Drs. Thomas J. Crevier and Jeffrey C. Yoder of Symyx for suggestions relating to the robotics experiments. The Bruker KAPPA APEXII X-ray diffractometer was purchased via an NSF CRIF: MU award to the California Institute of Technology, CHE-0639094.

Supporting Information Available: Selected ¹H NMR spectra, crystal and refinement data for **5m**, selected bond distances of **6**, and all CIFs. This material is available free of charge via the Internet at <http://pubs.acs.org>. CCDC 708866 (1), 713343 (2), 717612 (3), 711734 (4), 717605 (5), 723085 (**5m**), and 724780 (**6**) contain the supplementary crystallographic data for this paper. These data can be obtained free of charge from The Cambridge Crystallographic Data Centre via www.ccdc.cam.ac.uk/data_request/cif.

(19) Kliegman, J. M.; Barnes, R. K. *J. Org. Chem.* **1970**, *35*, 3140–3143.